The Astrophysical Journal Supplement Series, 264:37 (14pp), 2023 February https://doi.org/10.3847/1538-4365/aca65f

TESS Timings of 31 Hot Jupiters with Ephemeris Uncertainties

Su-Su Shan[1,2], Fan Yang[1,2,3], You-Jun Lu[1,2], Xing Wei[3], Wen-Wu Tian[1,2], Hai-Yan Zhang[1], Rui Guo[4], Xiao-Hong Cui[1], Ai-Yuan Yang[5], Bo Zhang[1,3], and Ji-Feng Liu[1,2,6]
[1] National Astronomical Observatories, Chinese Academy of Sciences, 20A Datun Road, Chaoyang District, Beijing 100101, People's Republic of China
sailoryf@nao.cas.cn, sailoryf1222@gmail.com, jfliu@nao.cas.cn
[2] School of Astronomy and Space Science, University of Chinese Academy of Sciences, Beijing 100049, People's Republic of China
[3] Department of Astronomy, Beijing Normal University, Beijing 100875, People's Republic of China
[4] Department of Astronomy, School of Physics and Astronomy, Shanghai Jiao Tong University, 800 Dongchuan Road, Shanghai 200240, People's Republic of China
[5] Max Planck Institute for Radio Astronomy, Auf dem Hügel 69, D-53121 Bonn, Germany
[6] WHU-NAOC Joint Center for Astronomy, Wuhan University, Wuhan, People's Republic of China
Received 2021 September 11; revised 2022 October 26; accepted 2022 November 22; published 2023 January 25

Abstract

A precise transit ephemeris serves as the premise for follow-up exoplanet observations. We compare TESS Object of Interest (TOI) transit timings of 262 hot Jupiters with the archival ephemeris and find 31 of them having TOI timing offsets, among which WASP-161b shows the most significant offset of -203.7 ± 4.1 minutes. The median value of these offsets is 17.8 minutes, equivalent to 3.6σ. We generate TESS timings in each sector for these 31 hot Jupiters, using a self-generated pipeline. The pipeline performs photometric measurements to TESS images and produces transit timings by fitting the light curves. We refine and update the previous ephemeris, based on these TESS timings (uncertainty $\sim$1 minute) and a long timing baseline ($\sim$10 yr). Our refined ephemeris gives the transit timing at a median precision of 0.82 minutes until 2025 and 1.21 minutes until 2030. We regard the timing offsets to mainly originate from the underestimated ephemeris uncertainty. All the targets with timing offset larger than 10σ present earlier timings than the prediction, which cannot be due to underestimated ephemeris uncertainty, apsidal precision, or Rømer effect as those effects should be unsigned. For some particular targets, timing offsets are likely due to tidal dissipation. Our sample leads to the detection of period-decaying candidates of WASP-161b and XO-3b reported previously.

Unified Astronomy Thesaurus concepts: Exoplanet astronomy (486); Exoplanet systems (484); Transit photometry (1709); Transit timing variation method (1710)

Supporting material: figure sets

1. Introduction

Transit ephemeris is crucial for exoplanet follow-up investigations, e.g., atmosphere analysis (Berta et al. 2012; Deming et al. 2013; Yang et al. 2021) and orbital evolution (Lendl et al. 2014; Dawson & Johnson 2018; Millholland & Laughlin 2018; Yee et al. 2020). The newly commissioned Transiting Exoplanet Survey Satellite (TESS; Ricker et al. 2015) provides precise timings in a long baseline when combined with previous works, which enables us to obtain a better transit ephemeris.

The observed transit timing could deviate from the ephemeris's prediction due to either the underestimation of ephemeris uncertainties (Mallonn et al. 2019), or physical processes (transit-timing variation, TTV; Agol & Fabrycky 2018). The TTV could originate from tidal dissipation, orbital precession, Rømer effect, mass loss, and multiple planets (Ragozzine & Wolf 2009; Lai et al. 2010; Mazeh et al. 2013; Patra et al. 2017; Agol & Fabrycky 2018; Yee et al. 2020; Bouma et al. 2020; Turner et al. 2021). For hot Jupiters, the interactions of planet companions are usually not massive or close enough to generate significant TTVs (Huang et al. 2016; Dawson & Johnson 2018).

TTV provides direct evidence of tidal dissipation that likely drives hot Jupiter migration (Dawson & Johnson 2018). WASP-12b has been reported to undergo tidal dissipation by observational TTVs (Patra et al. 2017; Yee et al. 2020; Turner et al. 2021). The TTVs are at the level of $\sim$5 minutes in a 10 yr baseline compared to the ephemeris obtained from a constant period (Yee et al. 2020). Apsidal precession is reported to be the primary explanation and seems to be ruled out with more than 10 yr of observations, including the most recent TESS timings (Patra et al. 2017; Yee et al. 2020; Turner et al. 2021). The referred works also discuss and exclude the other possible effects, including the Rømer effect and mass loss (Ragozzine & Wolf 2009; Lai et al. 2010).

The Rømer effect, i.e., the acceleration toward the line of sight, probably due to stellar companions, has been reported to dominate the TTV of WASP-4b (Bouma et al. 2020). Using TESS light curves, Bouma et al. (2019) present a period decreasing at -12.6 ± 1.2 ms yr^{-1}. Further radial-velocity (RV) monitoring indicates the Doppler effect contributes most of the period decreases (Bouma et al. 2020). For another example, WASP-53b and WASP-81b should harbor brown-dwarf companions that could cause TTVs $\sim$30 s, according to the calculation of Triaud et al. (2017).

We compare TESS timings and archival ephemeris predictions,[7] and report transit-timing offsets of 31 hot Jupiters in this work. The paper is organized as follows. We present the sample selection and data reduction in Section 2. In Section 3, transit timings and offsets compared to the previous ephemeris

[7] Exoplanet Archive: https://exoplanetarchive.ipac.caltech.edu/index.html.

are shown. The ephemeris refinement is also shown in this section. In Section 4, we discuss the possible physical origin of the timing offsets. We briefly summarize the work in Section 5.

2. Sample Selection and TESS Timing

The exoplanet sample in this work are hot Jupiters identified from previous work, and it has access to transit timings from the TESS Objects of Interest (TOI) Catalog (Guerrero et al. 2021). The archival data is extracted from the NASA Exoplanet Archive (Akeson et al. 2013; NASA Exoplanet Science Institute 2020).[8] The sample selection requires an orbital period of fewer than 10 days, a planet mass larger than 0.5 M_J, and a planet radius larger than 0.5 R_J. These criteria leave 421 hot Jupiters. After crossmatching this sample and the TOI catalog, we find that TESS observed and reported new transit timing for 262 hot Jupiters.

2.1. TESS Photometry and TOI Catalog

TESS was launched in 2018, possessing four cameras with a total field of view (FOV) of 24×96 square degrees, equivalent to a pixel resolution of 21″ (Ricker et al. 2015). The full-frame image (FFI) covering the FOV is released in a cadence of 30 minutes (as shown in Figure 1), while ∼200,000 targets are recorded with 11×11 pixel cutoff images in a cadence of 2 minutes (known as a target pixel file; TPF). The TESS data is available in MAST: 10.17909/t9-yk4w-zc73, 10.17909/t9-nmc8-f686.

The TOI catalog is built based on the light curves obtained from TESS image products, including both 2 minute and 30 minute frames (Guerrero et al. 2021). The 2 minute cadence light curve is generated by the Science Processing Operations Center (SPOC) pipeline and the 30 minute light curves by the Quick Look Pipeline (Twicken et al. 2016; Huang et al. 2020). Guerrero et al. (2021) generate an automated pipeline to derive transit parameters and thereby identify planet candidates with the method referred to as the Kepler Robovetter (Thompson et al. 2018). More than 2000 planet candidates (continuously being updated) are identified in the TOI catalog including both newly discovered and previously known planets.

The timing from the TOI catalog provides a long time baseline when compared with the previous ephemeris. The median timing baseline of the 262 exoplanets is 2368 days, while the median uncertainties of timings from archival data and from the TOI catalog are 0.59 and 0.84 minutes. The median uncertainty of archival periods is 4×10^{-6} days. 159 of 262 hot Jupiters show consistent TESS timings within 1σ when compared to the previous ephemeris predictions. This circumstantially demonstrates the accuracy of TOI timings. We neglect the difference between the barycentric Julian date (BJD) and heliocentric Julian date in this work. The difference is within ±4 s, beyond the timing precision discussed.

The TOI catalog has been well utilized for exoplanet research, including TTV analysis that uses the data in a similar condition to this work (Pearson 2019; Martins et al. 2020; Howard et al. 2021).

2.2. TESS Transit-timing Acquirement

A precision validation of TOI timing is necessary, for the purpose of the study on timing offsets to the previous ephemeris. A majority of the hot Jupiters (159 of 262) present consistent TOI timings, which could be circumstantial evidence. Direct evaluation is performed by independently reducing the data and obtaining the TESS timings. We generate a half-automatic pipeline to obtain and fit the light curve from TESS images (Yang et al. 2021, 2022a).

The pipeline includes two parts, i.e., a photometric pipeline and transit modeling. The photometric pipeline works on TESS image products (as shown in Figure 1) and includes modules, e.g., astrometry checking, aperture photometry, deblending of the nearby contamination flux, and light-curve detrending. The photometric pipeline generates light curves from raw images of both 30 minute cadence (FFI) and 2 minute cadence (TPF). During the TESS extended mission, the 30 minute cadence FFI is updated with a 10 minute cadence. The 10 minute FFI is used in our pipeline. Currently, we do not search for the recently released 20 s cadence data.

The photometric data reduction starts by finding if the TPF is available for the source. We would use the 2 minute cadence TPF for light-curve generation and the 30 minutes cadence FFI cutoff as a substitution when the TPF is not available. The astrometry would then be checked and corrected if there was any pointing jitter (Yang et al. 2021, 2022a). The astrometry check is based on the comparison between the nominal position reported by Gaia (Gaia Collaboration et al. 2018) and the target center in the TESS image. Circular aperture photometry is performed with a radius of 63″. The background is estimated as the median value of the lowest fifth percentile of pixel fluxes in the vicinity of the target. The photometry error is the quadratic sum of the Poisson error and the standard deviation of the background.

The flux contamination from nearby sources is modeled and removed using the flux profile as a function of the given center (Yang et al. 2022a). The detrending for long-term structure removal is performed by modeling the light curve of 0.6 days centering at the transit midpoint after masking the planetary transit. We use a linear function for modeling the long-term structure. We have tested with high-order polynomial functions (up to 10 orders) as well as a cubic spline function, which gives negligible differences for five validation targets in this work and the exoplanets investigated in previous works (Yang et al. 2021, 2021, 2022a).

The detrended light curve is performed with a stellar activity check from archival data and TESS photometry to avoid possible timing bias. The strong stellar activity would be taken into consideration. We note that the starspot perturbation is more significant to brightness than to the shape of the light curve unless the transit comes across the starspot (Makarov et al. 2009; Agol et al. 2010). Within the comparison sample in this work, we do not find any significant transits across starspots. Empirically, a Sunlike star would hold a variability at a level of ∼10 ppm on a planet-transit timescale (Jenkins 2002). In addition, the bias of timing estimation caused by starspots would be weakened by the detrending process.

More details and evaluations of the pipeline are referred to in previous works (Yang et al. 2021, 2022a). From the tests and applications so far, the derived transit parameters are within 1σ when we apply the same fitting to TPF light curves.

We derive timings of 31 hot Jupiters using our self-generated pipeline. And we check if the timing obtained from our pipeline is consistent with TOI timing and find the difference is commonly within 2 minutes. Comparison details are presented in Section 3.

[8] As of 2021 August.

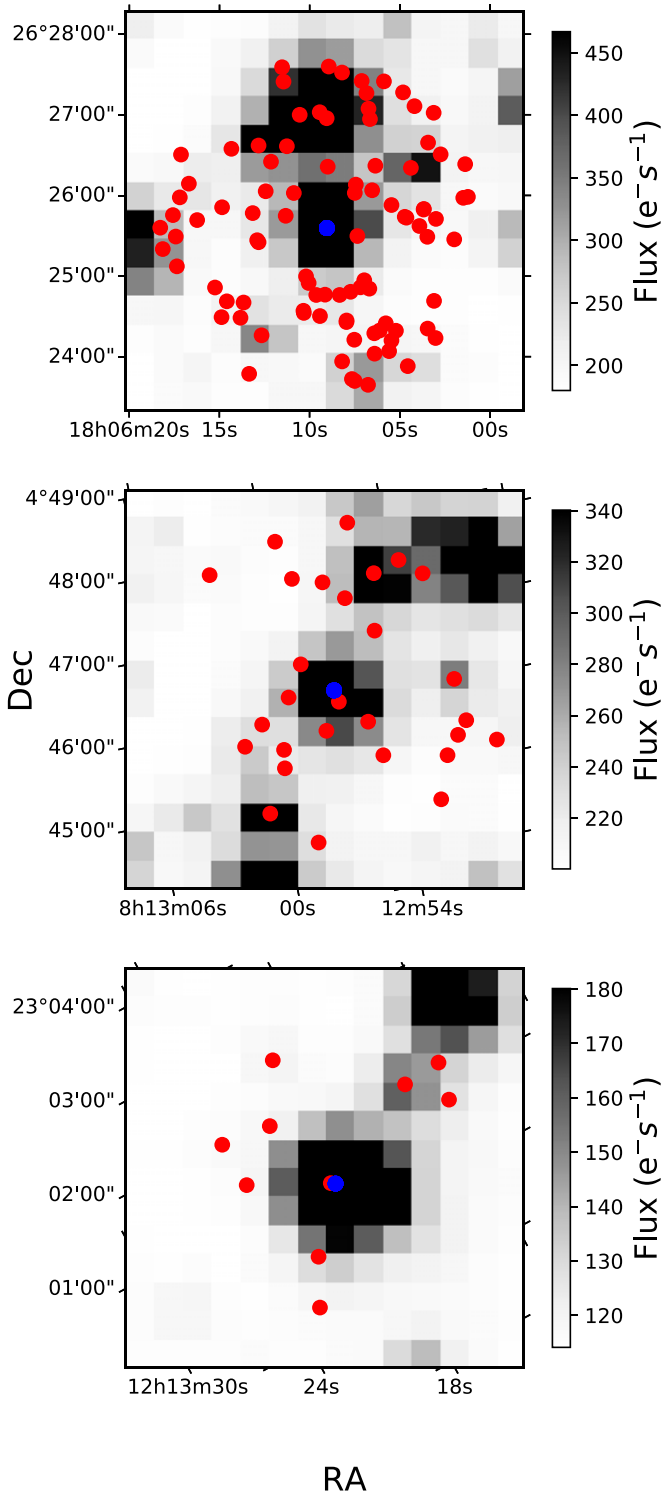

Figure 1. TESS example images of 14 × 14 pixels. The images correspond to HAT-P-31b, HAT-P-35b, and WASP-56b, from top to bottom. The blue points refer to the planet position in the Gaia catalog (Gaia Collaboration et al. 2018) while red points present nearby source positions.

Applying Markov Chain Monte Carlo (MCMC; Patil et al. 2010; Czesla et al. 2019), the light curve is fitted with a planet-transit model (Mandel & Agol 2002; Eastman et al. 2013). The choice of a *circular orbit* or a *Keplerian orbit* is consistent with the archival reference work. We briefly describe the transit modeling here with more details available in Yang et al. (2021, 2022a).

For circular orbit, the free parameters during our fitting are the transit midpoint (T_0), the ratio of the planet radius to the star radius (R_p/R_*), the semimajor axis (a/R_*), and the limb-darkening parameters. For the Keplerian orbit, the model has extra free parameters (during our fitting) of the longitude of the ascending node, the orbital eccentricity (e), the ascending node, the periapsis passage time, and the periapsis argument (ω). The fitting model as well as parameterization are taken from Eastman et al. (2013), e.g., formats of e and ω are $\sqrt{e}\ \sin\omega$ and $\sqrt{e}\ \cos\omega$.

The MCMC fitting runs 50,000 steps after an initial 50,000 steps as an initialization. All the priors are uniform, except for the limb darkening, which applies a Gaussian prior interpreted in a limb-darkening table (Claret 2018). We apply quadratic law (Sing 2010; Kipping 2013) for parameterizing limb darkening in this work. Specifically, the format is a standard parameterization of $u1$, $u2$. The uncertainty of the light curve applied for obtaining the MCMC final result is the standard deviation of the light-curve residual from an initial fitting. We do not apply a time-dependent term nor a jitter term for the uncertainty given that no significant evidence of time-dependent and jitter structures has been found during the previous TESS research experiences (Yang et al. 2021, 2021, 2022a; Yang & Wei 2022). We note that extra free parameters during fitting may reduce the fitting χ^2, which might be considered in future applications.

We apply the transit model to both the light curve of a single epoch and the light curve folded from one TESS sector (examples as shown in Figure 2). The folding is based on the archival ephemeris and we evaluate the fitting parameter bias if folding an inappropriate period (using the same method as in Yang et al. 2021). For one TESS sector, the timing bias is ∼4 minutes if the period is biased at 0.0004 days. Such a large period bias would cause significant TESS timing offsets when compared to ephemeris prediction and thereby is flagged. The fold-and-check method has been well utilized in period-searching studies (Schwarzenberg-Czerny 1989; Yang et al. 2020, 2021). In this work, we utilize and present the final timings obtained from folded light curves in one TESS sector. TOI timings are used for sample selection.

The oversampling technique is applied to mitigate influences caused by the sampling rate of TESS 30 minute data. Kipping (2010) reports on transit parameter bias caused by under-sampling and proposes the oversampling technique using a numerical solution to Kepler's equation. In previous work, we discussed the sampling influence on inclination and transit depth with and without the oversampling technique (Yang et al. 2022a). In this work, we check if the timing precision could improve using the oversampling technique. The median timing uncertainty is ∼4 minutes for modeling to the 30 minute cadence light curve without oversampling. The timing uncertainty is ∼1 minute for the 2 minute cadence light curve. Applying the oversampling routine from Kreidberg (2015), we resample the 30 minute light curve to the cadences of 1 minute, 2 minutes, and 10 minutes. The timing uncertainties obtained from fitting the resampled light curves are the same as the result when not applying the oversampling technique. We also test the oversampling to the 2 minute cadence light curve obtained from TPF. The resampling rate is set to be 0.5 and 1 minute. The test also yields a negligible timing difference. We note that the oversampling is particularly effective in estimating inclination as described in Yang et al. (2022a).

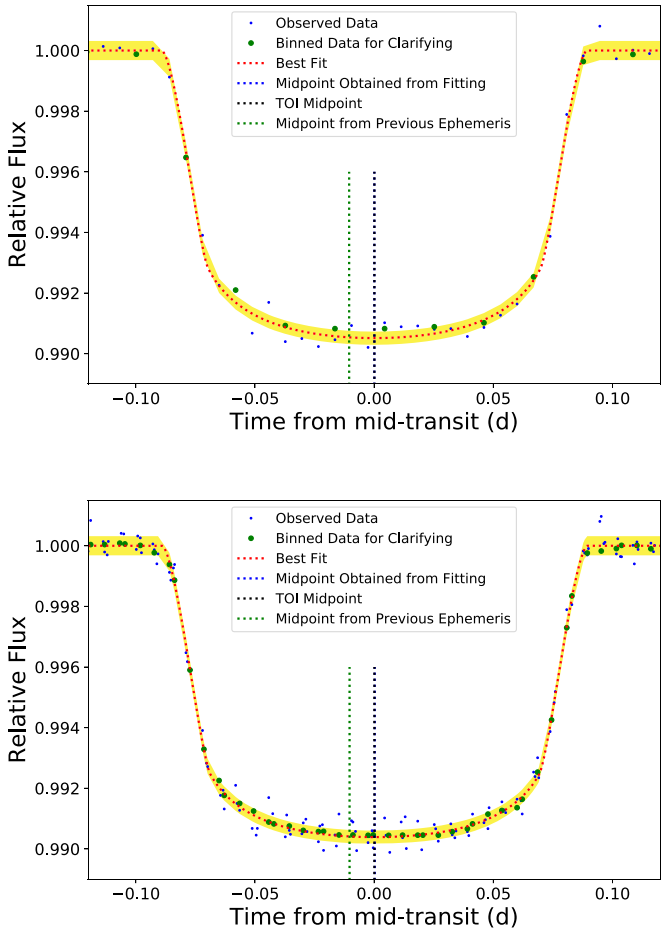

Figure 2. Light curves of KELT-19Ab as an example: a single epoch around TOI timing (top panel), folded multiple visits at a reference epoch (bottom panel). The blue points present observations (10 minute cadence) while the green points are bins of every three points for clarity. The red line gives the transit model fit with the yellow region indicating the 1σ confidence region. The vertical blue line gives the fitted timing; the black vertical line, TOI timing; the green vertical line, previous ephemeris prediction. The timings from single-epoch fitting (folded-epoch fitting) are only 0.14 minutes earlier (0.20 minutes later) than TOI, corresponding to a negligible difference as shown in the image (overlapped blue and black lines). The observed TESS timings show an offset of ∼15 minutes, compared to the previous ephemeris prediction as shown in the vertical green line. The fitting uncertainty is 0.54 minutes for a single epoch, and 0.23 minutes for folded epochs.

An extra timing uncertainty would be induced to be up to a few tenths of a minute for the 30 minute light curve. The FFI cutoff we use sets the time stamp as the same as the time of the FFI center. The timing difference during BJD to JD switching can be as large as 0.5 minutes for sources on the center of the CCD and on the $12^\circ \times 12^\circ$-sized corner of the CCD that TESS is at. This extra uncertainty is negligible considering the uncertainty of 4 minutes for timings obtained from the FFI cutoff. Two-minute light curves do not suffer such an issue as the time correction has been performed to TPF.

The median timing offset between our results and TOI timings is 1.43 minutes among the test sample. The median TOI timing uncertainty is 0.83 minutes. We conclude that it is reasonable to use TOI timings. And the TOI timing offset to the previous ephemeris is regarded as significant if the offset is larger than 4 minutes, which is ∼3 times the median difference. We also require the timing offset to be larger than 1 combined σ, which is the square root of the quadratic sum of archival ephemeris uncertainty and TESS timing uncertainty. These criteria lead to a final sample of 31 hot Jupiters.

3. Hot Jupiters with TESS Timing Offsets

We obtain a sample of 31 targets with TOI timing offsets compared to the previous ephemeris prediction. An example is shown in Figure 3 with the whole sample as shown in Figures A1–A3. The parameters are presented in Table 1, including planet ID, TESS time minus the predicted time from the previous ephemeris (ΔT_C), transit midpoint T_C, orbital period P, reduced chi-squared statistic ($\chi^2_{\rm red}$) of linear period fitting, category flag, and parameter reference. We take TOI timings as TESS timings when calculating ΔT_C and replace them with self-generated timings for WASP-173Ab, TOI-1333b, TOI-628b, KELT-21b, KELT-24b, and WASP-187b.

In our sample, the median ΔT_C is 17.8 minutes while the median combined uncertainty is 4.9 minutes. Therefore the signal-to-noise ratio (S/N) is 3.6. Among 31 hot Jupiters, WASP-161b presents the earliest offset timing of -203.7 ± 4.1 minutes. WASP-17b gives the latest offset timing of 70.8 ± 11.7 minutes. The timing uncertainty is derived as the quadratic sum of uncertainties of previous ephemerides and TESS timing.

We classify the sources into three categories, according to the potential properties implied by the timings. A type I target refers to a source whose timings are modeled with a linear function. The timing inconsistency could be either due to systematic error underestimation or some physical process. The linear function indicates a model with a constant derivative, referring to a constant period. Type II refers to the targets whose the timing differences cannot be modeled by a linear function, but by a quadratic function instead. The quadratic function can be due to abnormal points or physical processes that lead to a constant-period derivative. We identify the targets as type III if the timings cannot be fitted with any linear or quadratic functions. The possible physical origin of the timing offsets is discussed in Section 4.

Specifically, we present the reduced chi-squared ($\chi^2_{\rm red}$) statistic for type I targets if the data set number is larger than 2 (as shown in Table 1). We note that the limited number of data sets induces large uncertainty when calculating $\chi^2_{\rm red}$ (see details in Andrae et al. 2010). The Bayesian information criterion (BIC; details in Kass & Raftery 1995) difference for XO-3b is larger than 383, preferring a quadratic function to a linear fit (Yang & Wei 2022). We note that some hot Jupiters classified as type I may be better fitted with a quadratic function (e.g., WASP-161; Yang & Chary 2022), though the significance is not as high as XO-3b. These tentative signals need careful follow-up investigations and are not highlighted in this work.

We manually verify the TOI timings of 31 hot Jupiters among which WASP-173Ab, TOI-1333b, and TOI-628b need timing recalibration. We check the TESS raw data (2 minute cadence) of WASP-173Ab and find an abnormal data point around a transit at 2,468,356.564637 (BJD). The abnormal data biases the modeling if not clipped when performing an automatic pipeline. The points should be clipped if in excess of 10σ to the residual of successful transit fitting. We refit the TESS light curve with abnormal data having been clipped. The timing is $2{,}458{,}355.195662 \pm 0.00047$ (BJD) when we fit one transit visit and $2{,}458{,}355.195907 \pm 0.0001$ (BJD) when fitting visits folded through the whole sector. These two results are

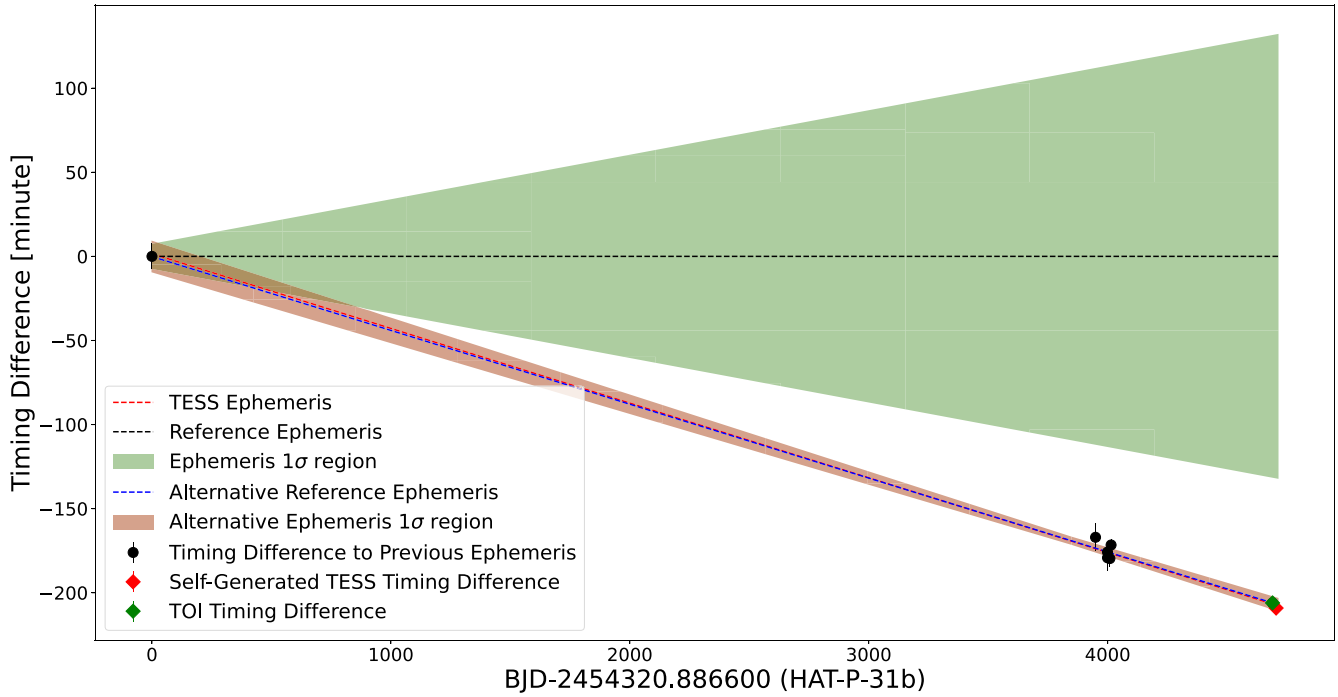

Figure 3. The timing difference of HAT-P-31b. The timing difference is the observed midtransit times minus the ephemeris predictions. The red point refers to the TESS timing difference, black points refer to timing differences of other observations from the literature (Kipping et al. 2011; Mallonn et al. 2019), the black dashed line is the reference ephemeris, the blue line is an alternative reference ephemeris, the red line is the refined ephemeris derived by combining TESS observations, the green region is a 1σ significant region of reference ephemeris, and the brown region is a 1σ significant region of alternative reference ephemeris. We note that our refined ephemeris overlaps the alternative reference ephemeris, indicating the consistency of the two ephemerides.

consistent within 0.35 minutes and are different from TOI timing at 29 minutes. The refitted TESS timing is consistent with the previous ephemeris (as shown in Figure 4).

TOI-1333b timing derived by refitting the TESS light curve is $2{,}458{,}715.1230 \pm 0.0010$ (BJD) which is 8.4 minutes later than TOI derived timing (as shown in Figure 4). The TESS 30 minute data (available for TOI-1333b) has some abnormal points around transits that would bias the timings if the sigma-clipping process was not applied. Removing the abnormal data points, we refit the light curve for the timing. The timings derived from a single transit and combined transits have a difference of 1.8 minutes (within 0.3 combined σ). The timing is close ($\sim 1\sigma$) to the prediction of the previous ephemeris (Figure 4).

We derive a combined timing of 1469.23270 ± 0.00222 (BJD) for TOI-628b while a single transit visit obtains a midpoint at 1469.2332 ± 0.0074 (BJD). The value is $\sim 1\sigma$ earlier than the TOI timing and is consistent with the previous ephemeris.

Comparing them with our generated TESS timings, TOI timings of KELT-21b, KELT-24b, and WASP-187b present differences of 10, 8, and 35 minutes, respectively. We note that TOI timings are highly reliable given that only five sources among 262 TOI hot Jupiters are found with possible issues, giving an error possibility of less than 2%.

3.1. Ephemeris Refinement

We refine the ephemeris of type I targets in our sample. We do not apply any ephemeris refinements to type II and III sources. The new ephemeris consists of TESS timings and a refined period (as shown in Table 1). The period is obtained from a linear fit of TESS timings and timings taken from archival papers (as listed in Table 2) as well as the Exoplanet Archive (Akeson et al. 2013). The refinement has a median precision of 0.82 minutes until 2025 and 1.21 minutes until 2030. The largest uncertainties are 34 minutes in 2025 and 61 minutes in 2030, coming from TOI-628b, due to the shortest baseline. Other than TOI-628b and TOI-1333b, all the refined timing uncertainties are within 5 minutes.

The ephemeris precision depends on the length of the time baseline and transit-timing precision. The timing uncertainties could be underestimated due to the techniques in light-curve generation and high-dimension model fitting (Yang et al. 2021, 2022a). Combined timing derived from multiple visits based on a constant-period assumption might be biased if the folding period is not precise, especially when the light curves partially cover the transits. Correcting the timing biases in archival papers (if present) is beyond the scope of this work.

The period could be updated when more observations are available (Mallonn et al. 2019; Edwards et al. 2021; Wang et al. 2021). The periods from the previous works are significantly different from the periods derived in our refinement. We note that these period differences might originate from physical processes, which makes the refinement inappropriate (as discussed in Section 4).

4. Discussion: Possible Physical Origin

Some targets in our sample present very significant period differences when compared to former results. It might not be a good hypothesis to regard all the differences as originating from the underestimation of archival period uncertainties. Period bias caused by a timing shift of 2 minutes would be only $\sim 10^{-5}$ days when the time baseline is 1 yr.

We argue that a very significant period difference might be attributed to physical period-changing processes. We find in our sample that the targets with an offset S/N larger than 10 all

Table 1
Exoplanet Parameters

Planet ID	ΔT_C (minutes)	T_c BJD	P (days)	$\chi^2_{\rm red}$	Category Flags	Reference
WASP-161b		2,458,492.286050 ± 0.00265	5.405366 ± 0.0000039	2.0419	I	This work; Yang & Chary (2022)
	−203.7 ± 4.1	2,459,249.035676 ± 0.000594				TOI timing
1		2,457,416.5289 ± 0.0011	5.4060425 ± 0.0000048			Barkaoui et al. (2019)
XO-3b		2,458,819.06428 ± 0.00035			II	This work; Yang & Wei (2022)
	−17.8 ± 1.2	2,458,819.064098 ± 0.000279				TOI Timing
1		2,455,292.43266 ± 0.00015	3.19153285 ± 0.00000058			Wong et al. (2014)
2		2,454,449.86816 ± 0.00023	3.1915239 ± 0.0000068			Winn et al. (2008)
		2,456,419.04365 ± 0.00026	3.19153247 ± 0.00000055			Wong et al. (2014)
KELT-18b		2,458,734.280341 ± 0.000335	2.871698 ± 0.0000004	2.7489	I	This work
		2,458,748.637347 ± 0.000331				
		2,458,906.582255 ± 0.000325				
		2,458,932.425443 ± 0.000353				
		2,459,624.505991 ± 0.000214				
		2,459,684.811712 ± 0.000239				
	−26.8 ± 2.3	2,458,714.181140 ± 0.000380				TOI timing
1		2,457,542.52504 ± 0.00039	2.8717518 ± 0.0000028			McLeod et al. (2017)
2		2,457,542.52463 ± 0.00057	2.8716992 ± 0.0000013			Maciejewski (2020)
WASP-54b		2,458,949.705160 ± 0.001171	3.693599 ± 0.0000006	0.8468	I	This work
		2,459,573.923274 ± 0.000538				
		2,459,669.955842 ± 0.000641				
	−55.9 ± 8.6	2,458,931.236409 ± 0.000435				TOI timing
1		2,455,518.35087 ± 0.00053	3.6936411 ± 0.0000059			Bonomo et al. 2017
K2-237b		2,458,642.067579 ± 0.001163	2.180535 ± 0.0000006	7.8139	I	This work
		2,459,387.806193 ± 0.000636				
	−15.5 ± 3.9	2,458,626.800781 ± 0.000869				TOI timing
1		2,457,656.4633789 ± 0.0000048	2.1805577 ± 0.0000057			Smith et al. (2019)
WASP-76b		2,459,133.976069 ± 0.000147	1.809881 ± 0.0000002	1.8398	I	This work
		2,459,472.424209 ± 0.000121				
		2,459,485.093248 ± 0.000136				
	−11.9 ± 2.9	2,459,117.687201 ± 0.000119				TOI timing
1		2,456,107.85507 ± 0.00034	1.809886 ± 0.000001			West et al. (2016)
WASP-95b		2,458,328.690567 ± 0.000287	2.184667 ± 0.0000002	1.1205	I	This work
		2,459,075.846388 ± 0.000132				
	−10.7 ± 2.9	2,459,084.585010 ± 0.000110				TOI timing
1		2,456,338.458510 ± 0.000240	2.184673 ± 0.0000014			Hellier et al. (2014)
WASP-101b		2,458,481.061101 ± 0.000185	3.585708 ± 0.0000003	4.4892 2	I	This work
		2,459,216.130731 ± 0.000145				
	−17.3 ± 5.2	2,459,223.302264 ± 0.000132				TOI timing
1		2,456,164.6934 ± 0.0002	3.585722 ± 0.000004			Hellier et al. (2014)
WASP-35b		2,458,459.092397 ± 0.000244	3.161569 ± 0.0000002	0.2758	I	This work
		2,459,179.930001 ± 0.000126				
	−9.5 ± 3.5	2,459,176.768453 ± 0.000197				TOI timing
1		2,455,531.479070 ± 0.000150	3.161575 ± 0.0000020			Enoch et al. (2011)
TOI-163b		2,458,350.038867 ± 0.000908	4.231119 ± 0.0000016	3.2752	I	This work
		2,458,371.194185 ± 0.001123				
		2,458,392.345356 ± 0.001497				
		2,458,421.969304 ± 0.000841				
		2,458,451.585295 ± 0.001530				
		2,458,481.204317 ± 0.000995				
		2,458,557.363318 ± 0.001196				
		2,458,574.287291 ± 0.000781				
		2,458,612.367794 ± 0.000928				
		2,458,629.292355 ± 0.001017				
		2,458,671.603439 ± 0.000874				

Table 1
(Continued)

Planet ID	ΔT_C (minutes)	T_c BJD	P (days)	$\chi^2_{\rm red}$	Category Flags	Reference
		2,459,039.709508 ± 0.000636				
		2,459,073.556184 ± 0.000635				
		2,459,069.328010 ± 0.000735				
		2,459,098.946501 ± 0.000611				
		2,459,132.796272 ± 0.000621				
		2,459,175.105352 ± 0.000618				
		2,459,204.723621 ± 0.000557				
		2,459,234.341314 ± 0.000575				
		2,459,263.960120 ± 0.000622				
		2,459,331.657993 ± 0.000505				
		2,459,348.581531 ± 0.000414				
		2,459,373.968750 ± 0.000331				
	−57.2 ± 22.0	2,459,310.502979 ± 0.000817				TOI timing
1		2,458,328.87970 ± 0.00063	4.231306 ± 0.000063			Kossakowski et al. (2019)
KELT-14b		2,458,493.272296 ± 0.000185	1.710054 ± 0.0000001	4.9021	I	This work
		2,459,202.944408 ± 0.000109				
		2,459,235.648287 ± 0.000969				
		2,459,235.435128 ± 0.000110				
	−10.7 ± 5.2	2,459,252.535529 ± 0.000108				TOI timing
1		2,457,091.028632 ± 0.000470	1.710059 ± 0.0000025			Rodriguez et al. (2016)
2		2,456,665.224010 ± 0.000210	1.710057 ± 0.0000032			Turner et al. (2016b)
KELT-7b		2,458,816.518431 ± 0.000430	2.734765 ± 0.0000002	3.3771	I	This work
		2,459,492.005468 ± 0.000231				
		2,459,519.352936 ± 0.000238				
		2,459,533.027055 ± 0.000234				
	−12.4 ± 5.4	2,458,819.253410 ± 0.000240				TOI timing
1		2,456,355.229809 ± 0.000198	2.734775 ± 0.0000039			Bieryla et al. (2015)
HAT-P-31b		2,459,025.840900 ± 0.001368	5.005269 ± 0.0000056	0.9519	I	This work
	−206.0 ± 131.6	2,459,010.826736 ± 0.001149				TOI timing
1		2,454,320.8866 ± 0.0052	5.005425 ± 0.000092			Kipping et al. 2011
2		2,458,169.9410 ± 0.0017	5.0052724 ± 0.0000063			Mallonn et al. (2019)
KELT-1b		2,458,765.534321 ± 0.000717	1.217494 ± 0.0000003	7.4954	I	This work
	−67.4 ± 53.9	2,458,765.533813 ± 0.000299				TOI timing
1		2,455,914.1628 ± 0.0023	1.217514 ± 0.000015			Siverd et al. (2012)
2		2,456,093.13464 ± 0.00019	1.21749448 ± 0.00000080			Baluev et al. (2015)
KELT-21b	−0.59 ± 2.5	2,458,690.462229 ± 0.000704	3.612769 ± 0.0000008	3.4411	I	This work
		2,458,719.364524 ± 0.000912				
		2,459,420.242127 ± 0.000267				
	−9.8 ± 2.4	2,458,686.841940 ± 0.000580				TOI timing
1		2,457,295.934340 ± 0.000410	3.612765 ± 0.0000030			Johnson et al. (2018)
HAT-P-69b		2,459,247.345980 ± 0.000274			III	This work
		2,458,510.155715 ± 0.000546				
	9.7 ± 1.5	2,459,242.559429 ± 0.000245				TOI timing
1		2,458,495.788610 ± 0.000720	4.786949 ± 0.0000018			Zhou et al. (2019)
WASP-17b		2,458,638.332379 ± 0.000340	3.735485 ± 0.0000003	5.5856	I	This work
		2,459,340.602164 ± 0.000403				
	70.8 ± 11.7	2,458,627.126221 ± 0.000584				TOI timing
1		2,454,559.181020 ± 0.000280	3.735442 ± 0.0000072			Anderson et al. (2010)
		2,454,577.85806 ± 0.00027	3.7354380 ± 0.0000068			Anderson et al. (2011)
		2,454,592.80154 ± 0.00050	3.7354845 ± 0.0000019			Southworth et al. (2012)
		2,457,192.69798 ± 0.00028	3.735438			Sedaghati et al. (2016)
WASP-178b		2,458,609.523699 ± 0.000421	3.344839 ± 0.0000007	3.4716	I	This work
		2,459,352.077016 ± 0.000181				
	12.9 ± 3.1	2,458,602.836430 ± 0.001860				TOI timing
		2,459,358.7671460 ± 0.0003877				TOI timing
1		2,456,927.068390 ± 0.000470	3.344829 ± 0.0000012			Hellier et al. (2019)
2		2,458,321.867240 ± 0.000380	3.344841 ± 0.0000033			

Table 1
(Continued)

Planet ID	ΔT_C (minutes)	T_c BJD	P (days)	$\chi^2_{\rm red}$	Category Flags	Reference
						Rodríguez Martínez et al. (2020)
WASP-33b		2,458,814.59179 ± 0.000193	1.219871 ± 0.0000001	4.8662	I	This work
	22.4 ± 6.9	2,458,791.414307 ± 0.000169				TOI timing
1		2,454,163.223730 ± 0.000260	1.219867 ± 0.0000012			Cameron et al. (2010)
2		2,455,507.522200 ± 0.000300	1.219868 ± 0.0000011			von Essen et al. (2014)
KELT-23Ab		2,458,701.953602 ± 0.000164			III	This work
		2,458,719.996122 ± 0.000187				
		2,458,758.335680 ± 0.000196				
		2,458,765.102458 ± 0.000197				
		2,458,895.908656 ± 0.000170				
		2,458,934.248842 ± 0.000181				
		2,459,443.943092 ± 0.000132				
		2,459,599.557734 ± 0.000131				
		2,459,613.090493 ± 0.000169				
		2,459,651.430016 ± 0.000135				
		2,459,669.472623 ± 0.000142				
		2,459,793.513154 ± 0.000138				
	23.8 ± 7.7	2,458,683.911214 ± 0.000056				TOI timing
1		2,458,140.379200 ± 0.002700	2.255251 ± 0.0000110			Johns et al. (2019)
2		2,458,140.386980 ± 0.000200	2.255288 ± 0.0000007			Maciejewski (2020)
HAT-P-6b		2,458,759.452299 ± 0.000648	3.852999 ± 0.0000004	7.5980	I	This work
		2,458,774.864299 ± 0.000681				
	26.3 ± 9.2	2,458,740.188710 ± 0.000360				TOI timing
1		2,454,035.675750 ± 0.000280	3.852985 ± 0.0000050			Noyes et al. (2008)
KELT-19Ab		2,459,222.7898588 ± 0.00020	4.611736 ± 0.0000009	4.1958	I	This work
		2,458,507.971344 ± 0.0002751				
	15.2 ± 5.9	2,459,222.789720 ± 0.000183				TOI timing
1		2,457,281.249537 ± 0.000361	4.611709 ± 0.0000088			Siverd et al. (2018)
WASP-94Ab		2,458,352.000206 ± 0.000642	3.950201 ± 0.0000006	0.5179	I	This work
		2,459,039.335697 ± 0.000323				
	10.2 ± 4.0	2,459,039.335846 ± 0.000386				TOI timing
1		2,456,416.402150 ± 0.000260	3.950191 ± 0.0000037			Bonomo et al. (2017)
WASP-58b		2,458,695.984265 ± 0.000376	5.017215 ± 0.0000005	2.7651	I	This work
		2,458,706.018411 ± 0.000428				
		2,458,991.998531 ± 0.000371				
		2,459,017.084690 ± 0.000379				
		2,459,413.444427 ± 0.000157				
		2,459,734.547119 ± 0.000164				
		2,459,764.650223 ± 0.000159				
	37.4 ± 13.5	2,458,986.981902 ± 0.000409				TOI timing
1		2,455,183.933500 ± 0.001000	5.017180 ± 0.0000110			Hébrard et al. (2013)
2		2,457,261.059700 ± 0.000620	5.017213 ± 0.0000026			Mallonn et al. (2019)
WASP-99b		2,458,393.713195 ± 0.000480	5.752591 ± 0.0000022	4.2045	I	This work
		2,459,112.785723 ± 0.000271				
		2,459,141.548814 ± 0.000244				
	61.6 ± 31.2	2,459,135.796019 ± 0.000239				TOI timing
1		2,456,224.983200 ± 0.001400	5.752510 ± 0.0000400			Bonomo et al. (2017)
TOI-1333b	2.67 ± 1.4	2,458,715.1230 ± 0.0010	4.720171 ± 0.0000204	0.0318	I	This work
		2,458,752.884599 ± 0.000828				
	−5.7 ± 1.5	2,458,715.117140 ± 0.000550				TOI timing
1		2,458,913.370330 ± 0.000450	4.720219 ± 0.0000110			Rodriguez et al. (2021)
WASP-78b		2,458,446.902114 ± 0.000472	2.175185 ± 0.0000003	3.9626	I	This work
		2,459,162.537455 ± 0.000227				
		2,459,192.991391 ± 0.000379				
	18.8 ± 11.1	2,459,175.589610 ± 0.000863				TOI timing

Table 1
(Continued)

Planet ID	ΔT_C (minutes)	T_c BJD	P (days)	$\chi^2_{\rm red}$	Category Flags	Reference
1		2,455,882.359640 ± 0.000530	2.175176 ± 0.0000047			Bonomo et al. (2017)
2		2,456,139.030300 ± 0.000500	2.175173 ± 0.0000030			Brown et al. (2017)
WASP-173Ab	1.2 ± 0.9	2,458,355.195662 ± 0.00047	1.386654 ± 0.0000006	0.3322	I	This work
	−30.4 ± 1.1	2,458,355.173660 ± 0.000620				TOI timing
1		2,457,288.8585 ± 0.0002	1.38665318 ± 0.00000027			Hellier et al. (2019)
2		2,458,105.59824 ± 0.00090	1.3866529 ± 0.0000027			Labadie-Bartz et al. (2019)
TOI-628b	3.8 ± 3.4	2,458,469.232700 ± 0.002220	3.409512 ± 0.0000335		I	This work
	7.4 ± 1.2	2,458,469.235200 ± 0.000430				TOI timing
1		2,458,629.479720 ± 0.000390	3.409568 ± 0.0000070			Rodriguez et al. (2021)
KELT-24b	1.0 ± 0.9	2,458,695.919325 ± 0.000633	5.551490 ± 0.0000011	1.7072	I	This work
		2,458,868.015428 ± 0.000148				
		2,458,895.773212 ± 0.000162				
		2,459,412.061344 ± 0.000102				
		2,459,423.164772 ± 0.000217				
		2,459,606.363810 ± 0.000204				
		2,459,617.467116 ± 0.000223				
	7.9 ± 0.9	2,458,684.821890 ± 0.000320				TOI timing
1		2,458,540.477590 ± 0.000360	5.551493 ± 0.0000081			Rodriguez et al. (2019)
2		2,458,268.454590 ± 0.000870	5.551492 ± 0.0000086			Maciejewski (2020)
WASP-187b	7.3 ± 8.7	2,458,785.428921 ± 0.001771	5.147885 ± 0.0000027		I	This work
	34.5 ± 8.7	2,458,764.856300 ± 0.002600				This work
1		2,455,197.352900 ± 0.002000	5.147878 ± 0.0000050			Schanche et al. (2020)

Note. "1" in column "Planet ID" indicates the reference ephemeris in Figures 3 and A1, while "2" presents the alternative ephemeris. The TESS timings derived by our pipeline are flagged as this work. The table is sorted by the significance of ΔT_C. Sources with earlier TESS timings are listed before the targets with later TESS timings.

present earlier observation timings. These sources are WASP-161b, XO-3b, and KELT-18b, among which WASP-161b and XO-3b are detected with clues of TTVs in our following work (Yang & Chary 2022; Yang & Wei 2022). The period difference caused by systematic underestimation should be unsigned, which is not the case. The tidal dissipation could explain the observational phenomenon.

The tidal torque transfers the energy between the star–planet orbit and the rotation of the star and planet (Goldreich & Soter 1966; Lin et al. 1996; Naoz et al. 2011; Wu & Lithwick 2011; Dawson & Johnson 2018; Rodet et al. 2021). The process could cause the period decay and the apsidal procession (Hut 1981; Ragozzine & Wolf 2009). The induced TTV has been discovered in WASP-12b at ∼a few minutes (Campo et al. 2011; Patra et al. 2017). And TESS provides the most recent evidence for the WASP-12b TTV (Turner et al. 2021).

We report on WASP-161b, which shows the most significant TESS timing offsets in this sample, presenting a period derivative ($\dot{P}$) of $-1.16 \times 10^{-7} \pm 2.25 \times 10^{-8}$ (as details described in Yang & Chary 2022). WASP-161b is possibly undergoing tidal dissipation. We have approved CHEOPS (Benz et al. 2021; Maxted et al. 2022) for two visit observations in 2022 for further investigation. WASP-161b is regarded as a type I target in this work.

The period of XO-3b has been reported differently in previous works (Johns-Krull et al. 2008; Winn et al. 2008, 2009; Wong et al. 2014; Bonomo et al. 2017, and references therein). TESS timing presents an offset of -17.8 ± 1.2 minutes (14.8σ) to the newest archival ephemeris from Bonomo et al. (2017). The timing generated by our pipeline is consistent within 0.3 minutes to TOI timing. And the uncertainties are similar (∼0.45 minutes). Yang & Wei (2022) report XO-3b as a tidal dissipation candidate by jointly analyzing archival timings and TESS timing.

The $\dot{P}$ is $-6.2 \times 10^{-9} \pm 2.9 \times 10^{-10}$ days per orbit per day, which relates to a timescale of orbital decay of 1.4 Myr. Applying equilibrium tide (Hut 1981; Leconte et al. 2010), Yang & Wei (2022) obtain a modified tidal quality factor $Q'_\star$ as $1.5 \times 10^5 \pm 6 \times 10^3$ if assuming the period decaying is due to the stellar tide. Q'_p is $1.8 \times 10^4 \pm 8 \times 10^2$ under the assumption that the period decaying is due to the planetary tide.

The number and properties of the detected dissipating planets would calibrate a series of crucial models in the planet formation theory, e.g., the dissipation as well as circularization timescale, and the possibility of capturing a floating planet or interacting with a stellar companion (Dawson & Johnson 2018).

The apsidal precession could be excited when the tidal torque exists (Ragozzine & Wolf 2009). To distinguish the difference between tidal dissipation and precession needs the modeling of timings of occultation (Patra et al. 2017; Yee et al. 2020; Turner et al. 2021). In previous work (Jordán & Bakos 2008; Antoniciello et al. 2021), XO-3b was also expected to be a candidate presenting precession. We note that the period variation originating from precession and the Rømer effect should be unsigned in the same way as from systematic underestimation.

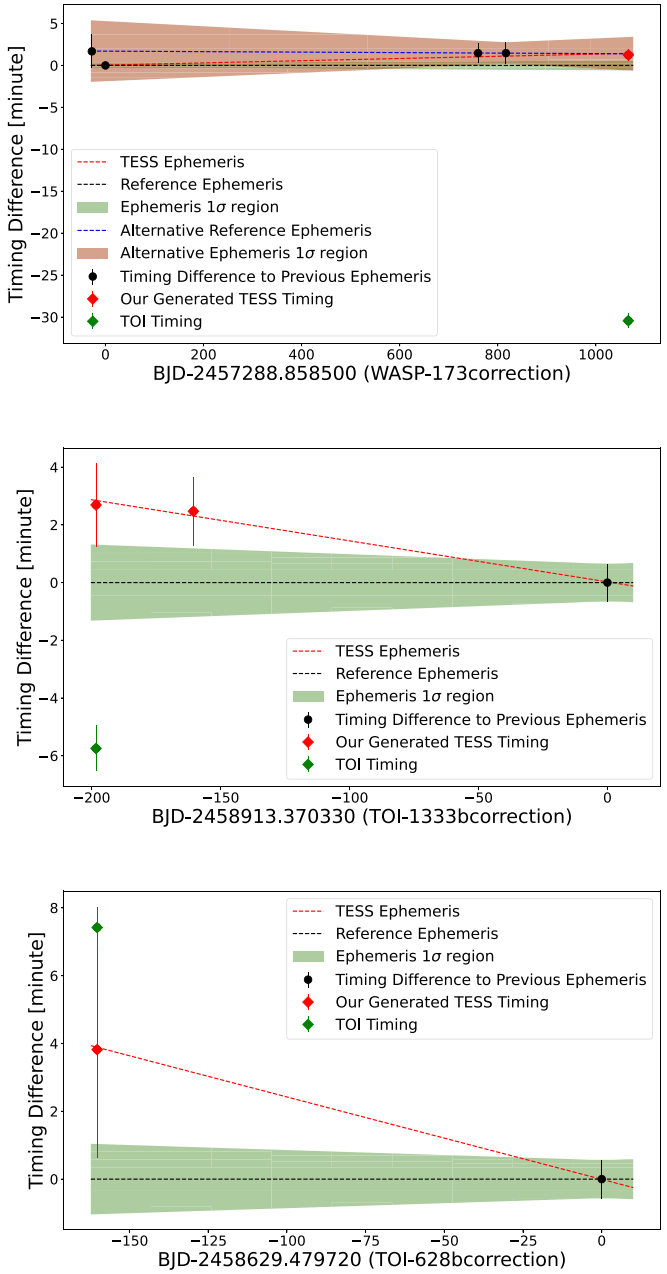

Figure 4. The timing differences with corrected timings for WASP-173Ab, TOI-1333b, and TOI-628b. The symbols are similar to Figure 3. The green diamonds indicate TOI timing and the red diamonds give the timing generated from TESS raw images.

The relation between the planet-period derivative and host-star acceleration rate is well modeled (Bouma et al. 2020). In our sample, KELT-19Ab shows a maximum stellar acceleration at 4 m s^{-1} yr^{-1} originating from the binary companion (Siverd et al. 2018). This acceleration would cause a period derivative of 5.32 ms yr^{-1}, according to the calculation from Bouma et al. (2020). We generated the TESS timings in both 2019 and 2020. The TOI catalog gives the timing in 2020, which is only 0.14 minutes different from our result (as shown in Figure 2 and the caption therein). We find timings can be fitted with both a linear and a quadratic function (as shown in Figure 5). The fitting result of the quadratic function indicates a period derivative of 112 ± 94 ms yr^{-1}. Therefore, we conclude that

Table 2
The Single Midtransit Times of Each Target from the Literature if Available

Planet ID	Midtransit Time T BJD_{TDB}	Reference
WASP-161b	2,458,492.286046 ± 0.00140	Yang & Chary (2022)
	2,458,497.690811 ± 0.00140	Yang & Chary (2022)
	2,458,508.501901 ± 0.00140	Yang & Chary (2022)
	2,458,513.908266 ± 0.00140	Yang & Chary (2022)
	2,459,232.818367 ± 0.00094	Yang & Chary (2022)
	2,459,238.225141 ± 0.00094	Yang & Chary (2022)
	2,459,243.629420 ± 0.00094	Yang & Chary (2022)
	2,459,249.035140 ± 0.00094	Yang & Chary (2022)
XO-3b	2,458,819.06428 ± 0.00035	Yang & Wei (2022)
	2,458,822.25556 ± 0.00034	Yang & Wei (2022)
	2,458,825.44732 ± 0.00037	Yang & Wei (2022)
	2,458,831.83008 ± 0.00035	Yang & Wei (2022)
	2,458,835.02191 ± 0.00034	Yang & Wei (2022)
	2,458,838.21397 ± 0.00042	Yang & Wei (2022)
	2,454,864.76684 ± 0.00040	Yang & Wei (2022)
	2,454,025.3967 ± 0.0038	Yang & Wei (2022)
	2,454,360.50866 ± 0.00173	Winn et al. (2008)
	2,454,382.84500 ± 0.00265	Winn et al. (2008)
	2,454,382.84523 ± 0.00112	Winn et al. (2008)
	2,454,392.41999 ± 0.00130	Winn et al. (2008)
	2,454,395.61179 ± 0.00167	Winn et al. (2008)
	2,454,398.80332 ± 0.00066	Winn et al. (2008)
	2,454,411.56904 ± 0.00161	Winn et al. (2008)
	2,454,449.86742 ± 0.00067	Winn et al. (2008)
	2,454,465.82610 ± 0.00038	Winn et al. (2008)
	2,454,478.59308 ± 0.00119	Winn et al. (2008)
	2,454,481.78455 ± 0.00070	Winn et al. (2008)
	2,454,507.31319 ± 0.00118	Winn et al. (2008)
	2,454,513.69768 ± 0.00090	Winn et al. (2008)
KELT-18b	$2{,}457{,}493.70451^{+0.00082}_{-0.00084}$	McLeod et al. (2017)
	2,457,493.7064 ± 0.0011	McLeod et al. (2017)
	$2{,}457{,}493.7046^{+0.00086}_{-00.00087}$	McLeod et al. (2017)
	$2{,}457{,}496.5787^{+0.0017}_{-0.0018}$	McLeod et al. (2017)
	2,457,539.6551 ± 0.0017	McLeod et al. (2017)
	2,457,545.3962 ± 0.0011	McLeod et al. (2017)
	2,457,559.7568 ± 0.0011	McLeod et al. (2017)
	2,457,559.7572 ± 0.0020	McLeod et al. (2017)
	$2{,}457{,}559.7536^{+0.0019}_{-0.0020}$	McLeod et al. (2017)
	$2{,}457{,}588.4709^{+0.0014}_{-0.0013}$	McLeod et al. (2017)
	$2{,}457{,}591.3461^{+0.0015}_{-0.0016}$	McLeod et al. (2017)
K2-237b	2,458,589.73380 ± 0.00061	Edwards et al. (2021)
KELT-14b	2,457,043.146899 ± 0.000775	Rodriguez et al. (2016)
	2,457,048.276707 ± 0.000961	Rodriguez et al. (2016)
	2,457,091.027548 ± 0.001076	Rodriguez et al. (2016)
	2,457,091.033997 ± 0.001551	Rodriguez et al. (2016)
	2,457,091.027674 ± 0.001400	Rodriguez et al. (2016)
	2,457,103.002776 ± 0.001377	Rodriguez et al. (2016)
	2,457,111.550157 ± 0.001956	Rodriguez et al. (2016)
	2,457,114.965950 ± 0.001308	Rodriguez et al. (2016)
	2,457,771.62839 ± 0.00035	Edwards et al. (2021)
	2,457,783.59845 ± 0.00044	Edwards et al. (2021)
	2,458,544.57156 ± 0.00061	Edwards et al. (2021)
KELT-7b	2,456,204.817057 ± 0.000741	Bieryla et al. (2015)
	2,456,223.959470 ± 0.000358	Bieryla et al. (2015)
	2,456,234.898861 ± 0.000486	Bieryla et al. (2015)
	2,456,245.839584 ± 0.000579	Bieryla et al. (2015)
	2,456,254.045118 ± 0.000730	Bieryla et al. (2015)
	2,456,270.451621 ± 0.000637	Bieryla et al. (2015)
	2,456,319.678871 ± 0.000683	Bieryla et al. (2015)

Table 2
(Continued)

Planet ID	Midtransit Time T BJD_{TDB}	Reference
	2,456,322.413721 ± 0.000648	Bieryla et al. (2015)
	2,456,584.950978 ± 0.000544	Bieryla et al. (2015)
	2,456,680.667558 ± 0.001007	Bieryla et al. (2015)
HAT-P-31b	2,458,270.05094 ± 0.00564	Mallonn et al. (2019)
	2,458,320.09907 ± 0.00131	Mallonn et al. (2019)
	2,458,320.09673 ± 0.00550	Mallonn et al. (2019)
	2,458,330.10726 ± 0.00340	Mallonn et al. (2019)
	2,458,335.11829 ± 0.00213	Mallonn et al. (2019)
KELT-1b	2,455,899.5549 ± 0.0010	Siverd et al. (2012)
	2,455,899.55408 ± 0.00044	Siverd et al. (2012)
	$2,455,905.63860^{+0.00084}_{-0.00082}$	Siverd et al. (2012)
	2,455,911.72553 ± 0.00045	Siverd et al. (2012)
	$2,455,927.55574^{+0.00040}_{-0.00042}$	Siverd et al. (2012)
	$2,455,933.64320^{+0.00041}_{-0.0003}$	Siverd et al. (2012)
KELT-21b	2,456,898.527802 ± 0.001956	Johnson et al. (2018)
	2,456,956.337374 ± 0.001053	Johnson et al. (2018)
	2,457,588.567597 ± 0.000775	Johnson et al. (2018)
	2,457,624.696694 ± 0.000799	Johnson et al. (2018)
	2,457,624.695694 ± 0.000833	Johnson et al. (2018)
	2,457,624.693194 ± 0.000694	Johnson et al. (2018)
	2,457,902.879452 ± 0.000775	Johnson et al. (2018)
	2,457,902.879181 ± 0.000521	Johnson et al. (2018)
	2,459,033.67650 ± 0.00032	Garai et al. (2022)
	2,459,051.74102 ± 0.00071	Garai et al. (2022)
	2,459,055.35200 ± 0.00021	Garai et al. (2022)
	2,459,087.86668 ± 0.00046	Garai et al. (2022)
WASP-17b	2,453,890.549230 ± 0.004306	Anderson et al. (2010)
	2,453,905.482660 ± 0.003819	Anderson et al. (2010)
	2,453,920.423160 ± 0.0025	Anderson et al. (2010)
	2,453,965.238059 ± 0.003472	Anderson et al. (2010)
	2,454,200.571537 ± 0.003056	Anderson et al. (2010)
	2,454,215.522667 ± 0.001875	Anderson et al. (2010)
	2,454,271.557737 ± 0.002847	Anderson et al. (2010)
	2,454,286.494817 ± 0.005764	Anderson et al. (2010)
	2,454,301.452058 ± 0.005694	Anderson et al. (2010)
	2,454,331.323827 ± 0.006458	Anderson et al. (2010)
	2,454,555.437350 ± 0.004444	Anderson et al. (2010)
	2,454,566.651190 ± 0.005764	Anderson et al. (2010)
	2,454,592.801221 ± 0.000382	Anderson et al. (2010)
	2,456,423.18973 ± 0.00023	Alderson et al. (2022)
	2,456,426.9246 ± 0.0003	Alderson et al. (2022)
	2,457,921.1177278 ± 0.000775	Alderson et al. (2022)
	2,457,958.473652 ± 0.000775	Alderson et al. (2022)
	2,456,367.15615529 ± 0.001615	Alderson et al. (2022)
	2,456,086.99426107 ± 0.001615	Alderson et al. (2022)
	2,456,370.8921914 ± 0.001499	Alderson et al. (2022)
WASP-33b	2,452,984.82964 ± 0.00030	Turner et al. (2016a)
	2,456,029.62604 ± 0.0001624	Zhang et al. (2018)
	2,456,024.74659 ± 0.00014	Zhang et al. (2018)
	2,456,878.65777 ± 0.00033	Maciejewski et al. (2018)
	2,456,900.61530 ± 0.00036	Maciejewski et al. (2018)
	2,457,753.30433 ± 0.00052	Maciejewski et al. (2018)
	2,457,764.28369 ± 0.00043	Maciejewski et al. (2018)
	2,458,015.57583 ± 0.00046	Maciejewski et al. (2018)
	2,458,026.55466 ± 0.00077	Maciejewski et al. (2018)
	2,458,075.35041 ± 0.00037	Maciejewski et al. (2018)
	2,458,381.53678 ± 0.00055	Maciejewski et al. (2018)
	2,458,403.49659 ± 0.00045	Maciejewski et al. (2018)
	2,458,430.33394 ± 0.00056	Maciejewski et al. (2018)
	2,458,436.43219 ± 0.00034	Maciejewski et al. (2018)
KELT-23Ab	2,458,144.898400 ± 0.000463	Johns et al. (2019)
	2,458,144.897240 ± 0.000440	Johns et al. (2019)
	2,458,153.917930 ± 0.000590	Johns et al. (2019)
	2,458,153.916810 ± 0.000949	Johns et al. (2019)
	2,458,167.448400 ± 0.001100	Johns et al. (2019)
	2,458,187.745830 ± 0.000637	Johns et al. (2019)
	2,458,196.770350 ± 0.001100	Johns et al. (2019)
	2,458,196.771060 ± 0.000625	Johns et al. (2019)
	2,458,196.773500 ± 0.001192	Johns et al. (2019)
	2,458,273.452490 ± 0.000984	Johns et al. (2019)
	2,458,302.769970 ± 0.000810	Johns et al. (2019)
HAT-P-6b	2,454,347.76763 ± 0.00042	Szabo et al. (2010)
	2,454,698.3908 ± 0.0011	Szabo et al. (2010)
	2,454,740.77668 ± 0.00063	Todorov et al. (2012)
	2,455,160.75292 ± 0.00034	Todorov et al. (2012)
	2,455,430.4657 ± 0.0013	Todorov et al. (2012)
KELT-19Ab	2,457,073.723660 ± 0.001042	Siverd et al. (2018)
	2,457,087.554255 ± 0.001412	Siverd et al. (2018)
	2,457,101.393149 ± 0.001887	Siverd et al. (2018)
	2,457,405.764653 ± 0.000521	Siverd et al. (2018)
	2,457,405.766335 ± 0.000683	Siverd et al. (2018)
	2,457,405.768490 ± 0.000995	Siverd et al. (2018)
	2,457,405.766362 ± 0.000822	Siverd et al. (2018)
	2,457,728.584553 ± 0.001042	Siverd et al. (2018)
WASP-58b	2,455,183.9342 ± 0.0010	Mallonn et al. (2019)
	2,456,488.40790 ± .00264	Mallonn et al. (2019)
	2,456,498.44187 ± 0.00121	Mallonn et al. (2019)
	2,456,523.52545 ± 0.00316	Mallonn et al. (2019)
	2,456,528.54704 ± 0.00134	Mallonn et al. (2019)
	2,457,120.57537 ± 0.00297	Mallonn et al. (2019)
	2,457,637.35161 ± 0.0008975	Mallonn et al. (2019)
	2,457,968.48759 ± 0.00068141	Mallonn et al. (2019)
	2,457,968.48541 ± 0.00082141	Mallonn et al. (2019)
	2,458,259.48221 ± 0.00249199	Mallonn et al. (2019)
WASP-173Ab	$2,457,261.1266^{+0.0013}_{-0.0014}$	Labadie-Bartz et al. (2019)
	$2,458,048.74546^{+0.00084}_{-0.00078}$	Labadie-Bartz et al. (2019)
	$2,458,105.59824^{+0.00090}_{-0.00084}$	Labadie-Bartz et al. (2019)

combining TESS and archival timings does not present a significant TTV dominated by stellar acceleration for KELT-19Ab. We regard the Rømer effect as beyond the detection limit in this work.

Further investigation requires long-term measurements with both photometric and spectroscopic instruments. The trend of

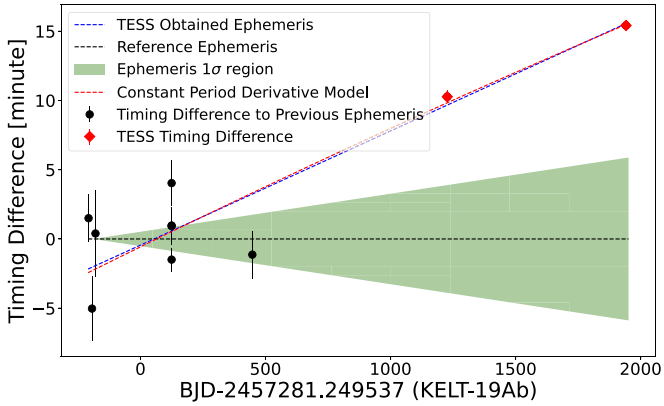

Figure 5. KELT-19Ab timings fitted with a quadratic function. The symbols are similar to Figure 3. The red line shows the quadratic function model.

the RV curve if present indicates stellar companions (Bouma et al. 2020). Modeling timing evolution reveals TTV evidence (Holman et al. 2010; Patra et al. 2017; Yang & Wei 2022). Approved telescope proposals have proved to be effective in analyzing the timing offsets of hot Jupiters (Ragozzine & Wolf 2009; Patra et al. 2017). Sky surveys, e.g., Kepler and TESS, provide more light curves for timing analysis (Borucki et al. 2011; Ivshina & Winn 2022). Moreover, the sample for relevant analysis can be potentially extended by upcoming time-domain surveys, e.g., the Large Synoptic Survey Telescope (LSST; Lund et al. 2015a) and SiTian (Liu et al. 2021; Yang et al. 2022b).

5. Summary

We discuss the ephemeris of 31 hot Jupiters, of which TOI timings show offsets. We refine the ephemeris of the sample by jointly fitting TESS timings and archival times from previously published papers. The TESS timings are obtained by our self-generated pipeline. The pipeline obtains the light curve from the raw TESS images and fits the light curve with the planet-transit model. The result from our pipeline gives consistent results compared to the TOI catalog.

Within the sample, TOI timings present a median offset of 17.8 ± 4.9 minutes, equivalent to an S/N of 3.6σ when compared to the previous ephemeris. WASP-161b and XO-3b give the most significant timing offsets. The ephemeris refinement serves potential for follow-up observations with the latest equipment, e.g., CHEOPS, and those ongoing with the James Webb Space Telescope and the Ariel Space Telescope. The refined timing reaches a precision within 0.82 minutes in the next 5 yr and 1.21 minutes in the next 10 yr.

WASP-161b, XO-3b, and KELT-18b present timing offsets larger than 10σ. These three targets all have an earlier observed timing than the predictions from the previous ephemeris under a constant-period assumption. We find WASP-161b and XO-3b present evidence of period decaying (Yang & Chary 2022; Yang & Wei 2022). Apsidal precession could be an alternative explanation to the TTVs. Interestingly, all four targets (WASP-161, XO-3b, WASP-12b, and WASP-4b) reported with observed TTVs show earlier timing than the prediction in a constant-period model. Apsidal precession could not explain this since the timing variation caused by precession should be unsigned. Further observations, e.g., occultation timing monitoring, are helpful for confirmation.

This work made use of the NASA Exoplanet Archive[9] (Akeson et al. 2013) and PyAstronomy[10] (Czesla et al. 2019). We would like to thank Ranga-Ram Chary for the helpful discussions. S.-S.S., F.Y., and J.-F.L. acknowledge funding from the National Key Research and Development Program of China (No. 2016YFA0400800), the National Natural Science Foundation of China (NSFC; No. 11988101), the CSST Milky Way and Nearby Galaxies Survey on Dust and Extinction Project (CMS-CSST-2021-A09) and the Cultivation Project for LAMOST Scientific Payoff and Research Achievement of CAMS-CAS. H.-Y.Z. acknowledges NSFC (Nos. 12041301, U1831128). X. W. is supported by NSFC (Nos. 11872246, 12041301), and the Beijing Natural Science Foundation (No. 1202015).

Appendix

Figures A1–A3 show the timing differences of 31 targets classified by three types. The complete set of targets for Figures A1 and A3 are available in the online figure sets.

[9] https://exoplanetarchive.ipac.caltech.edu/index.html
[10] https://github.com/sczesla/PyAstronomy

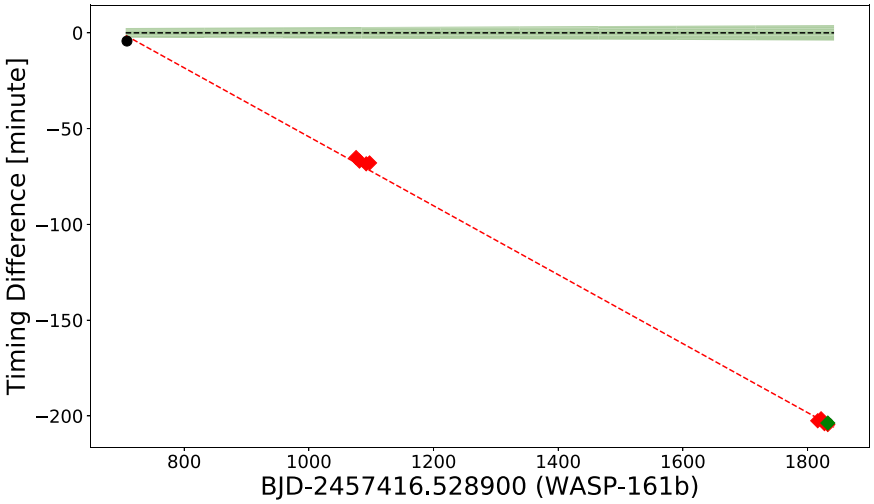

Figure A1. Timing differences of Type I targets of which the timings can be fitted by a linear function. The symbols are the same as in Figure 3 and the legend inside the image is dismissed for clarity.

(The complete figure set (28 images) is available.)

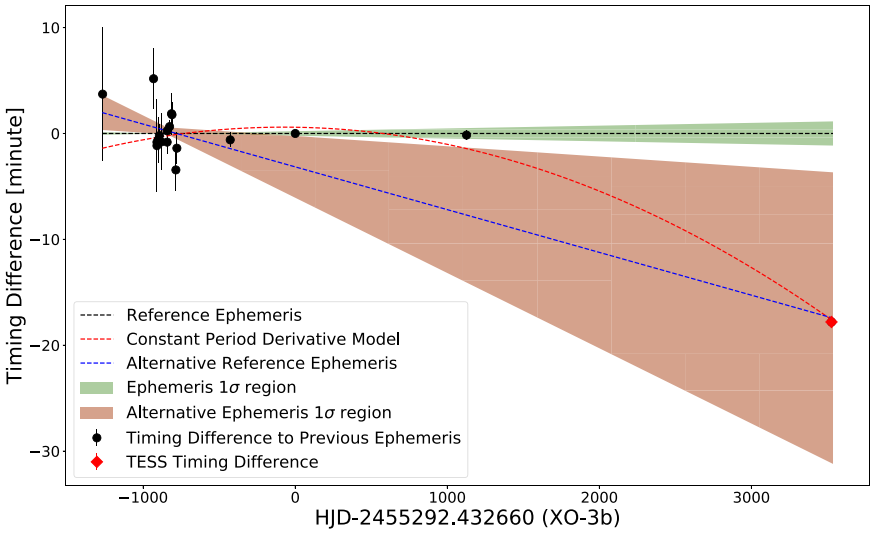

Figure A2. Timing differences of Type II targets of which timings would be modeled by a quadratic function.

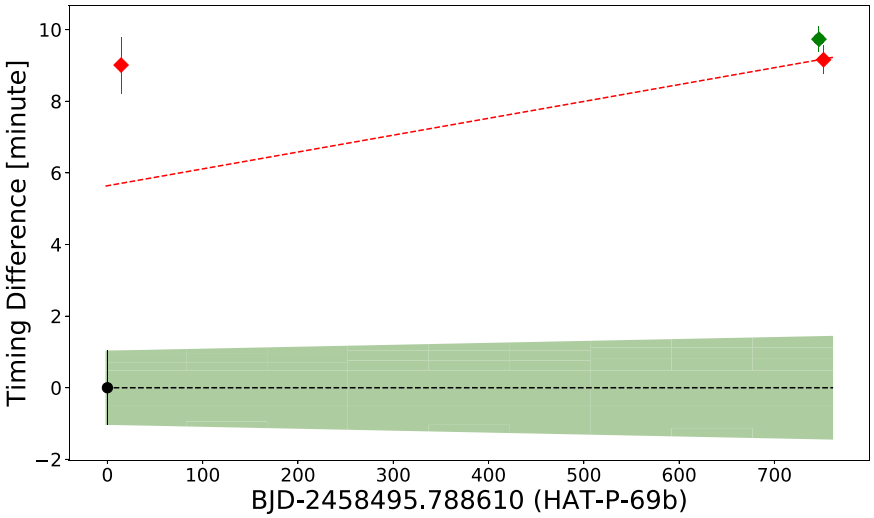

Figure A3. Timing differences of Type III targets of which the timings cannot be fitted with any linear or quadratic functions.

(The complete figure set (2 images) is available.)

ORCID iDs

Su-Su Shan https://orcid.org/0000-0002-5744-2016
Fan Yang https://orcid.org/0000-0002-6039-8212
You-Jun Lu https://orcid.org/0000-0002-1310-4664
Xing Wei https://orcid.org/0000-0002-8033-2974
Wen-Wu Tian https://orcid.org/0000-0002-9079-7556
Xiao-Hong Cui https://orcid.org/0000-0002-6322-7582
Bo Zhang https://orcid.org/0000-0002-6434-7201
Ji-Feng Liu https://orcid.org/0000-0002-2874-2706

References

Agol, E., Cowan, N. B., Knutson, H. A., et al. 2010, ApJ, 721, 1861
Agol, E., & Fabrycky, D. C. 2018, in Handbook of Exoplanets, ed. H. J. Deeg & J. A. Belmonte (Berlin: Springer), 7
Akeson, R. L., Chen, X., Ciardi, D., et al. 2013, PASP, 125, 989
Alderson, L., Wakeford, H. R., MacDonald, R. J., et al. 2022, MNRAS, 512, 4185
Anderson, D. R., Hellier, C., Gillon, M., et al. 2010, ApJ, 709, 159
Anderson, D. R., Smith, A. M. S., Lanotte, A. A., et al. 2011, MNRAS, 416, 2108
Andrae, R., Schulze-Hartung, T., & Melchior, P. 2010, arXiv:1012.3754
Antoniciello, G., Borsato, L., Lacedelli, G., et al. 2021, MNRAS, 505, 1567
Baluev, R. V., Sokov, E. N., Shaidulin, V. S., et al. 2015, MNRAS, 450, 3101
Barkaoui, K., Burdanov, A., Hellier, C., et al. 2019, AJ, 157, 43
Benz, W., Broeg, C., Fortier, A., et al. 2021, ExA, 51, 109
Berta, Z. K., Charbonneau, D., Désert, J.-M., et al. 2012, ApJ, 747, 35
Bieryla, A., Collins, K., Beatty, T. G., et al. 2015, AJ, 150, 12
Bonomo, A. S., Desidera, S., Benatti, S., et al. 2017, A&A, 602, A107
Borucki, W. J., Koch, D. G., Basri, G., et al. 2011, ApJ, 736, 19
Bouma, L. G., Winn, J. N., Baxter, C., et al. 2019, AJ, 157, 217
Bouma, L. G., Winn, J. N., Howard, A. W., et al. 2020, ApJL, 893, L29
Brown, D. J. A., Triaud, A. H. M. J., Doyle, A. P., et al. 2017, MNRAS, 464, 810
Cameron, A. C., Guenther, E., Smalley, B., et al. 2010, MNRAS, 407, 507
Campo, C. J., Harrington, J., Hardy, R. A., et al. 2011, ApJ, 727, 125
Claret, A. 2018, A&A, 618, A20
Czesla, S., Schröter, S., Schneider, C. P., et al. 2019, PyA: Python astronomy-related packages, Astrophysics Source Code Library, ascl:1906.010
Dawson, R. I., & Johnson, J. A. 2018, ARA&A, 56, 175
Deming, D., Wilkins, A., McCullough, P., et al. 2013, ApJ, 774, 95
Eastman, J., Gaudi, B. S., & Agol, E. 2013, PASP, 125, 83
Edwards, B., Changeat, Q., Yip, K. H., et al. 2021, MNRAS, 504, 5671
Enoch, B., Anderson, D. R., Barros, S. C. C., et al. 2011, AJ, 142, 86
Gaia Collaboration, Brown, A. G. A., Vallenari, A., et al. 2018, A&A, 616, A1
Garai, Z., Pribulla, T., Kovács, J., et al. 2022, MNRAS, 513, 2822
Goldreich, P., & Soter, S. 1966, Icar, 5, 375
Guerrero, N. M., Seager, S., Huang, C. X., et al. 2021, ApJS, 254, 39
Hébrard, G., Collier Cameron, A., Brown, D. J. A., et al. 2013, A&A, 549, A134
Hellier, C., Anderson, D. R., Bouchy, F., et al. 2019, MNRAS, 482, 1379
Hellier, C., Anderson, D. R., Cameron, A. C., et al. 2014, MNRAS, 440, 1982
Holman, M. J., Fabrycky, D. C., Ragozzine, D., et al. 2010, Sci, 330, 51
Howard, W. S., Teske, J., Corbett, H., et al. 2021, AJ, 162, 147
Huang, C., Wu, Y., & Triaud, A. H. M. J. 2016, ApJ, 825, 98
Huang, C. X., Vanderburg, A., Pál, A., et al. 2020, RNAAS, 4, 204
Hut, P. 1981, A&A, 99, 126
Ivshina, E. S., & Winn, J. N. 2022, ApJS, 259, 62
Jenkins, J. M. 2002, ApJ, 575, 493
Johns, D., Reed, P. A., Rodriguez, J. E., et al. 2019, AJ, 158, 78
Johns-Krull, C. M., McCullough, P. R., Burke, C. J., et al. 2008, ApJ, 677, 657
Johnson, M. C., Rodriguez, J. E., Zhou, G., et al. 2018, AJ, 155, 100
Jordán, A., & Bakos, G. Á. 2008, ApJ, 685, 543
Kass, R. E., & Raftery, A. E. 1995, J. Am. Stat. Assoc., 90, 773
Kipping, D. M. 2010, MNRAS, 408, 1758
Kipping, D. M. 2013, MNRAS, 435, 2152
Kipping, D. M., Hartman, J., Bakos, G. Á., et al. 2011, AJ, 142, 95
Kossakowski, D., Espinoza, N., Brahm, R., et al. 2019, MNRAS, 490, 1094
Kreidberg, L. 2015, PASP, 127, 1161
Labadie-Bartz, J., Rodriguez, J. E., Stassun, K. G., et al. 2019, ApJS, 240, 13
Lai, D., Helling, C., & van den Heuvel, E. P. J. 2010, ApJ, 721, 923
Leconte, J., Chabrier, G., Baraffe, I., & Levrard, B. 2010, A&A, 516, A64
Lendl, M., Triaud, A. H. M. J., Anderson, D. R., et al. 2014, A&A, 568, A81
Lin, D. N. C., Bodenheimer, P., & Richardson, D. C. 1996, Natur, 380, 606
Liu, J., Soria, R., Wu, X.-F., Wu, H., & Shang, Z. 2021, An. Acad. Bras. Ciênc., 93, 20200628
Lund, M. B., Pepper, J., & Stassun, K. G. 2015a, AJ, 149, 16
Maciejewski, G. 2020, AcA, 70, 181
Maciejewski, G., Fernández, M., Aceituno, F., et al. 2018, AcA, 68, 371
Makarov, V. V., Beichman, C. A., Catanzarite, J. H., et al. 2009, ApJL, 707, L73
Mallonn, M., von Essen, C., Herrero, E., et al. 2019, A&A, 622, A81
Mandel, K., & Agol, E. 2002, ApJL, 580, L171
Martins, B. L. C., Gomes, R. L., Messias, Y. S., et al. 2020, ApJS, 250, 20
Maxted, P. F. L., Ehrenreich, D., Wilson, T. G., et al. 2022, MNRAS, 514, 77
Mazeh, T., Nachmani, G., Holczer, T., et al. 2013, ApJS, 208, 16
McLeod, K. K., Rodriguez, J. E., Oelkers, R. J., et al. 2017, AJ, 153, 263
Millholland, S., & Laughlin, G. 2018, ApJL, 869, L15
Naoz, S., Farr, W. M., Lithwick, Y., Rasio, F. A., & Teyssandier, J. 2011, Natur, 473, 187
NASA Exoplanet Science Institute 2020, Planetary Systems Table, IPAC doi:10.26133/NEA12
Noyes, R. W., Bakos, G. Á., Torres, G., et al. 2008, ApJL, 673, L79
Patil, A., Huard, D., & Fonnesbeck, C. J. 2010, JSS, 35, 1
Patra, K. C., Winn, J. N., Holman, M. J., et al. 2017, AJ, 154, 4
Pearson, K. A. 2019, AJ, 158, 243
Ragozzine, D., & Wolf, A. S. 2009, ApJ, 698, 1778
Ricker, G. R., Winn, J. N., Vanderspek, R., et al. 2015, JATIS, 1, 014003
Rodet, L., Su, Y., & Lai, D. 2021, ApJ, 913, 104
Rodriguez, J. E., Colón, K. D., Stassun, K. G., et al. 2016, AJ, 151, 138
Rodriguez, J. E., Eastman, J. D., Zhou, G., et al. 2019, AJ, 158, 197
Rodriguez, J. E., Quinn, S. N., Zhou, G., et al. 2021, AJ, 161, 194
Rodríguez Martínez, R., Gaudi, B. S., Rodriguez, J. E., et al. 2020, AJ, 160, 111
Schanche, N., Hébrard, G., Collier Cameron, A., et al. 2020, MNRAS, 499, 428
Schwarzenberg-Czerny, A. 1989, MNRAS, 241, 153
Sedaghati, E., Boffin, H. M. J., Jeřabková, T., et al. 2016, A&A, 596, A47
Sing, D. K. 2010, A&A, 510, A21
Siverd, R. J., Beatty, T. G., Pepper, J., et al. 2012, ApJ, 761, 123
Siverd, R. J., Collins, K. A., Zhou, G., et al. 2018, AJ, 155, 35
Smith, A. M. S., Csizmadia, S., Gandolfi, D., et al. 2019, AcA, 69, 135
Southworth, J., Hinse, T. C., Dominik, M., et al. 2012, MNRAS, 426, 1338
Szabo, G. M., Haja, O., Szatmary, K., Pal, A., & Kiss, L. L. 2010, IBVS, 5919, 1
Thompson, S. E., Coughlin, J. L., Hoffman, K., et al. 2018, ApJS, 235, 38
Todorov, K. O., Deming, D., Knutson, H. A., et al. 2012, ApJ, 746, 111
Triaud, A. H. M. J., Neveu-VanMalle, M., Lendl, M., et al. 2017, MNRAS, 467, 1714
Turner, J. D., Pearson, K. A., Biddle, L. I., et al. 2016a, MNRAS, 459, 789
Turner, J. D., Ridden-Harper, A., & Jayawardhana, R. 2021, AJ, 161, 72
Turner, O. D., Anderson, D. R., Collier Cameron, A., et al. 2016b, PASP, 128, 064401
Twicken, J. D., Jenkins, J. M., Seader, S. E., et al. 2016, AJ, 152, 158
von Essen, C., Czesla, S., Wolter, U., et al. 2014, A&A, 561, A48
Wang, X.-Y., Wang, Y.-H., Wang, S., et al. 2021, ApJS, 255, 15
West, R. G., Hellier, C., Almenara, J.-M., et al. 2016, A&A, 585, A126
Winn, J. N., Holman, M. J., Torres, G., et al. 2008, ApJ, 683, 1076
Winn, J. N., Johnson, J. A., Fabrycky, D., et al. 2009, ApJ, 700, 302
Wong, I., Knutson, H. A., Cowan, N. B., et al. 2014, ApJ, 794, 134
Wu, Y., & Lithwick, Y. 2011, ApJ, 735, 109
Yang, F., & Chary, R.-R. 2022, AJ, 164, 259
Yang, F., Chary, R.-R., & Liu, J.-F. 2022a, AJ, 163, 42
Yang, F., Long, R. J., Liu, J.-f., et al. 2021, AJ, 161, 294
Yang, F., Long, R. J., Shan, S.-S., et al. 2020, ApJS, 249, 31
Yang, F., Shan, S.-S., Guo, R., et al. 2021, Ap&SS, 366, 83
Yang, F., Wang, W., Wei, X., et al. 2022b, RAA, 22, 055005
Yang, F., & Wei, X. 2022, PASP, 134, 024401
Yang, F., Zhang, B., Long, R. J., et al. 2021, ApJ, 923, 226
Yee, S. W., Winn, J. N., Knutson, H. A., et al. 2020, ApJL, 888, L5
Zhang, M., Knutson, H. A., Kataria, T., et al. 2018, AJ, 155, 83
Zhou, G., Huang, C. X., Bakos, G. Á., et al. 2019, AJ, 158, 141